Effect of the Fermi surface destruction on transport properties in underdoped cuprates

Jian-Xin Li*
Institute of Physics, Academia Sinica, Taipei 11529, Taiwan

W.C. Wu
Institute of Physics, Academia Sinica, Taipei 11529, Taiwan
and Department of Physics, National Taiwan Normal University, Taipei 11718, Taiwan

T.K. Lee
Institute of Physics, Academia Sinica, Taipei 11529, Taiwan
and National Center for Theoretical Sciences, P.O.Box 2-131, Hsinchu, Taiwan

Motivated by recent experimental measurements on the Fermi surface(FS) destruction in underdoped high-T_c cuprates, we examine its effect on the transport properties based on the Boltzmann equation approach. The effect is modeled by simply taking the density of states for electrons in the gapped regions to be zero. Within the nearly antiferromagnetic Fermi liquid model, we calculate the temperature dependences of the dc resistivity, the inverse Hall angle and the Hall coefficient. It is shown that the effect of the FS destruction on transport properties is sensitive to the existance and the range of the flat band near $(0, \pm\pi)$ in the dispersion of electrons, and the anistropy of the relaxation rate along the Fermi surface. We find that the experimental data are better described by the cold spot model, i.e., the transports are determined mainly by the contribution of the electrons near the Brillouin-zone diagonals.

PACS number: 74.72.-h, 74.25.Fy, 72.15.Gd

I. INTRODUCTION

Normal state transports in high-T_c cuprates continue to be a challenging subject. It is known for a long time that the resistivity $\rho(T)$ in the normal state shows a linear temperature behavior down to the superconducting transition temperature T_c and meanwhile the inverse Hall angle $\cot\theta_H(T)$ and the Hall coefficient $R_H(T)$ have T^2 and T^{-1} temperature dependences, respectively. However, the situation is different in underdoped systems, in which both $\rho(T)$ and $R_H(T)$ deviate from their high-T behaviors below certain temperatures higher than T_c [1,2].

Various models have been proposed to accout for the temperature behaviors of the resistivity, the inverse Hall angle as well as the Hall coefficient [3]. Among them, of accumulating interest is the models based on the so-called hot spots and/or cold spots [4–7], which refer to small regions on the Fermi surface(FS) where the electron lifetime is unusually short or long, respectively. Fundamentally, in this kind of models, the anomalous temperature dependences of transport coefficients are ascribed to the anistropy of scatterings on different momentum regions. Some successes have been achieved based on these models. However, there are relatively few studies of the transport properties in underdoped cuprates. One of the striking features in underdoped high-T_c cuprates is that there is a normal state gap (pseudogap) as measured by various experiments [8]. Recent angle-resolved photoemission(ARPES) experiment [9] further indicates that the pseudogap opens up at different momentum points at different temperatures, consequently it leads to a FS composed of disconnected arcs in the pseudogap state. Because the electron lifetime varies over the Fermi surface as assumed in the hot spot and/or cold spot models and also as suggested by ARPES experiments [10,11], it is expected that the losing of some parts of FS will affect its temperature behavior. It is our aim in this paper to study the effects of the destruction of the FS on the transport properties in the pseudogap state. Our main results are: (1) Based on the standard Boltzmann transport theory, we demonstrate that the transport properties in the pseudogap state are well described by the cold spot model— the main contribution to transports comes from the cold spots and the hot spots contribute little, which is consistent with the recent studies on the transports in the normal state [3,6]. (2) For the realistic calculations using the nearly antiferromagnetic Fermi liquid (NAFL) interaction form [3,5,12], we find that the variation of the Fermi velocity along the FS is an essential ingredient for the justification of the applicability of the cold spot model. (3) The bandstructure which has an extended flat band near $(0, \pi)$ gives a good account for the experimental observations. (4) By reducing the dispersion for optimally doped high-T_c cuprates by a factor of 3, we can fit our result for the resistivity with experiments quantitatively. Moreover, using the same parameters, we find that the calculated temperature dependence of the inverse Hall angle is also consistent with the experimental data [2]. As for the Hall coefficient, we get a weaker temperature dependence than experiments, however its crossover behavior from the normal to the pseudogap state is in agreement with experiments qualitatively.

The paper is organized as follows. In Section II, we discuss the effect of the variation of the Fermi velocity along the FS on the resistivity in the pseudogap state by comparing two kinds of tight-binding bandstructures which differ in the flatness of the dispersions near $(0, \pm\pi)$ points. In Section III, we present fits to experimental data of the resistivity and the inverse Hall angle and discuss qualitatively the crossover behavior of the Hall coefficient from the normal to the pseudogap state. Section IV contains a brief discussion and a conclusion.

II. EFFECT OF THE VARIATION OF FERMI VELOCITY ON RESISTIVITY

Currently, the most commonly used band structure for quasiparticles in high-T_c cuprates is the two-dimensional tight-binding model including the neast- and next-neast- neighbour hopping term which is written as,

$$\varepsilon_k = -2t(\cos k_x + \cos k_y) - 4t^{'} \cos k_x \cos k_y - \mu, \tag{1}$$

where, $t = 0.25$eV, $t^{'}/t = -0.45$ and μ is the chemical potential which is determined by hole concentration. As will be discussed below, we find that this dispersion fails to account for the temperature dependence of the resistivity in the pseudogap state as far as our model is concerned. Thus, another bandstructure is also considered, which is obtained by a tight-binding fit to ARPES energy dispersion by Norman *et al.* [9]. It reads,

$$\begin{aligned}\varepsilon_k = t_0 + t_1(\cos k_x + \cos k_y) + t_2 \cos k_x \cos k_y + t_3(\cos 2k_x + \cos 2k_y) \\ +t_4(\cos 2k_x \cos k_y + \cos 2k_y \cos k_x) + t_5 \cos 2k_x \cos 2k_y - \mu,\end{aligned} \tag{2}$$

with real space hopping matrix elements (in eV) $[t_0, ..., t_5]$= [0.1305,-0.2976,0.1636,-0.026,-0.0559,0.051]. Experimentally, the pseudogap opens at different temperatures for different hole doping concentrations. However, since the opening temperature T^* is chosen by hand in our model, this change can be naturally realized. Thus, we will not consider the effect of different doping levels and fix the hole concentration $n = 0.1$. The FS's for these two dispersions corresponding to $n = 0.1$ are shown in Fig.1. The main difference between them is that the energy band Eq.(2) is flatter near the crossing of the FS and the Brillouin zone boundary. This difference can be seen more clearly from their dispersions plotted in Fig.2. As shown, a very flat band exists near the M point along the direction of Γ to M for Eq.(2). Consequently, the Fermi velocity at k-point A for the dispersion (2) is nearly 2.5 times smaller than at k-point B(A and B are indicated in Fig.1), while it varies slightly for the dispersion (1), as one can see from the inset of Fig.2. In the following, we will see that this slight difference affects the temperature behavior of the transport coefficients in the pseudogap state qualitatively. It is worthy to point out that both dispersions are obtained by fitting to the ARPES experiments on the optimally doped materials. So, applying them to underdoped systems by just adjusting the chemical potential is a rigid band approximation. Because no detailed bandstructure for underdoped materials is available for us now, we will use this approximation in this section for a qualitative discussion on the sensitivity of the resistivity in the pseudogap state with respect to the variation of the Fermi velocity along the FS. In section IV, we will demonstrate that this assumption fails to fit to the experimental data quantitatively and the best fit to experiments is the dispersion (2) reduced by a factor of 3.

Though there are many studies for the origin of this pseudogap [13], no consensus seems to have been achieved. The ARPES experiments show that the gap has a $d_{x^2-y^2}$ symmetry and it first appears near $(0, \pm\pi)$ and $(\pm\pi, 0)$ points, the gapped regions spread laterally on cooling the samples [9]. In the presence of gap, the transfer rates of electrons into and out of these regions as well as the excitations of electrons in these regions will drop rapidly. For simplicity, here we assume that the states in the gapped region(shown schematically in Fig.1 as the regions closed by four bold line semi-circles) is unavailable for electrons. These regions first appear at the opening temperature of the pseudogap and will extend gradually as temperature decreases. Because only several ARPES data on the destruction of the FS are available, we can not deduce a precise form of its variation as a function of temperature and will assume that the T-dependences of the radius of the gapped regions will be $R(T) \propto (T^* - T)$, $R(T) \propto (T^* - T)^{1/2}$ and $R(T) \propto \tanh 2\sqrt{(T^*/T) - 1}$ (T^* the opening temperature of the pseudogap) and its maximum value at the superconducting transition temperature T_c be $R_{max} = 0.3\pi$ (the case of $R_{max} = 0.25\pi$ is sometimes also included for comparison). We will choose $T^* = 150$K and T_c =64K to fit to the experimental data on $YBa_2Cu_3O_{6+x}$. Our model is reminiscent of a recent proposal by Furukawa, Rice and Salmhofer [14]. Based on the one-loop renormalation group investigation, they demonstrated that the FS with saddle points $(\pi, 0)$ and $(0, \pi)$ can be truncated by the formation of an insulting condensate due to the umklapp scattering as the electron density increases, while the remaining FS is still metallic. It also bears a close similarity to the bosonic preformed pairs model by Geshkenbein, Ioffe and Larkin [15], in which the fermions lying inside the disks shown in Fig.1 are assumed to be paired into dispersionless bosons, and the interaction of transferring electrons from the disks to other parts of the FS is weak so that the bosons are in fact localized.

In order to proceed the detail calculations, a form of the effective interaction between electrons and spin fluctuations is required. We note that, the anisotropy of scatterings on the Fermi line can be naturally realized in the nearly antiferromagnetic Fermi liquids(NAFL) model [3,5,12], where the spin fluctuations strongly peak at the AF wave vector (π, π). So, we will adopt this model interaction which reads [3,5,12],

$$\chi(\mathbf{q}, \omega) = \sum_i \frac{1}{\omega_{q_i} - i\omega} \tag{3}$$

where $\omega_{q_i} = T^c + \alpha T + \omega_D \psi_{q_i}$, $\psi_{q_i} = 2 + \cos(q_x + \delta Q_i) + \cos(q_y)$(or $2 + \cos(q_x) + \cos(q_y + \delta Q_i)$), T^c, α, and ω_D are temperature-independent parameters. The sum over i runs over the incommensurate wavevector $\delta Q_i = \pm 0.12\pi$, which has been shown to exist in $YBa_2Cu_3O_{6.6}$ [16], recently. In our discussion, the results with commensuration $\delta Q_i = 0$ are also included for comparison.

We assume that a weak magnetic field is applied perpendicular to the CuO_2 plane and an electrical field is along the x direction, i.e., $\mathbf{E} = E\mathbf{e_x}$ and $\mathbf{B} = B\mathbf{e}_z$. Within the conventional relaxation-time approximation, the longitudinal and Hall conductivities can be calculated according to,

$$\sigma_{xx} = -2e^2 \sum_k [\mathbf{v}(k) \cdot \mathbf{e_x}]^2 \tau_k [\frac{\partial f(\varepsilon_k)}{\partial \varepsilon_k}], \tag{4}$$

$$\sigma_{xy} = -2e^3 \sum_k [\mathbf{v}(k) \cdot \mathbf{e_x} \tau(k)] \mathbf{v}(k) \times \mathbf{B} \cdot \nabla [\mathbf{v}(k) \cdot \mathbf{e_y} \tau(k)] [\frac{\partial f(\varepsilon_k)}{\partial \varepsilon_k}], \tag{5}$$

where, $\mathbf{v}(k) = \nabla_{\mathbf{k}} \varepsilon_k$ is the group velocity and $\tau(k)$ the relaxation time.

Following Stojkovic and Pines [3], we will approximate the relaxation rates by the electron lifetime. To second-order in the interaction constant g, it reads,

$$\frac{1}{\tau(k)} = 2g^2 \sum_{k'} \mathrm{Im}\chi(k - k', \varepsilon_{k'} - \varepsilon_k)[n(\varepsilon_{k'} - \varepsilon_k) + f(\varepsilon_{k'})], \tag{6}$$

where $n(\varepsilon)$ and $f(\varepsilon)$ are the Bose and Fermi distribution functions, respectively.

We solve Eqs.(4), (5) and (6) numerically by dividing the Brillouin zone into 200×200 lattices. The parameters for the spin-fluctuation spectrum are choosen as $T^c = 0$, $\alpha = 2.0$ and $\omega_D = 77$meV. Another set of parameters, namely, $T^c = 0$, $\alpha = 2.0$ and $\omega_D = 147$meV [12] is also used, no qualitative change has been found. The interaction constant is taken to be $g = 0.64eV$ as used before [12]. In the pseudogap state, the sum over $k(k')$ in Eqs.(4), (5) and (6) will exclude those regions where the gap is formed.

The temperature dependences of the relaxation rates τ_k for both dispersions are presented in Fig.3. Due to the opening of the pseudogap, a decrease is observed for all cases at low temperatures. This result is expected because we have taken the density of states in the gapped region to be zero after the temperature is lower than the opening temperature $T^* = 150$K. We note that the gapped regions first appear at $(0, \pm\pi)$ points and the energy difference between the chemical potential and that at $(0, \pm\pi)$ is 1950 K and 650 K for the dispersions (1) and (2), respectively, at the same doping concentration $n = 0.1$. Because transports involve the scatterings of electrons situating about several KT around the FS, the destruction of the FS affects the transport properties only when the difference between the energies at the FS and at the gapped regions is comparable with KT. As a result, the decrease in $1/\tau_k$ starts at different temperatures for the dispersions (1) and (2). It starts at nearly T^* for the dispersion (1)(shown in (c) and (d)) and at lower temperature for the dispersion (2)(shown in (a) and (b)), especially it will depends on the spreading rate of the gapped regions for the dispersion (2). Comparing $1/\tau_k$ at different k-points A and B, one finds that the relaxation rate is strongly anistropy along the FS, it is larger near the hot spots such as the k-point A and smaller near the cold spots such as k-point B. This is due to the anistropy of the interaction form Eq.(3). We would like to emphasize that there is no appreciable difference in the ratios of the $1/\tau_k$ at hot spots to at cold spots calculated using the dispersions (1) and (2), namely it is about 4 for the dispersion (1) and 7 for the dispersion (2).

Now, we turn to the discussion of the dc resistivity. Before proceeding with a detail analysis, one may speculate that the resistivity will decrease once the temperature is below T^*(or the temperature when $1/\tau_k$ starts to decrease for the dispersion (2)) as inferred from the behavior of $1/\tau_k$, according to the well-known Drude formular for resistivity $\rho = m^*/(n_e e^2 \tau)$ (here τ is an effective relaxation rate, m^* the effective mass and n_e the number of electrons). However, the numerical result for $\rho(T) = 1/\sigma_{xx}$ calculated using Eq.(4) turns out to be not so trivial, since the quantity m^*/n_e will change after parts of the FS is destroyed due to the formation of the pseudogap. As shown in Fig.4(a), the dc resistivity calculated using the dispersion (1) goes up instead of going down after the gap opens for all cases of R_{max}

and $R(T)$, which contradicts the experimental observation [1], while those calculated using the dispersion (2) (as shown in Fig.4(b)) show a decrease below T^* though a small rise can also be observed below about 100 K and 80 K for the cases of $R_{max} = 0.3\pi$, $R(T) \propto (T^* - T)$, and $R_{max} = 0.25\pi$, $R(T) \propto \tanh 2\sqrt{(T^*/T) - 1}$, respectively. Since the relaxation rate at the cold spots shows decrease once entering into the pseudogap state, the contribution to the longitudinal conductivity from the cold spots $\sigma_{xx}^{(c)}$ will increase. On the other hand, the density of states near the hot spots will lose because of the opening of pseudogap and it gives rise to a decrease in the conductivity coming from the hot spots $\sigma_{xx}^{(h)}$. Therefore, whether the resistivity rises or drops in the pseudogap state depends on the competition of the increment in $\sigma_{xx}^{(c)}$ and the decrease in $\sigma_{xx}^{(h)}$. For the cold spot model in which the relaxation rate at the hot spots is assumed to be unusually larger than at the cold spots [3,6], $\sigma_{xx}^{(h)}$ will be short-circuited and the conductivity σ_{xx} is determined by $\sigma_{xx}^{(c)}$. So, σ_{xx} will increase and in turn the resistivity $\rho(T) = 1/\sigma_{xx}$ will decrease. To the contrary, for the hot spot model [7] the contribution from the hot spots is comparable with or even larger than that from the cold spots, then the decrease in $\sigma_{xx}^{(h)}$ will surpass the increase in $\sigma_{xx}^{(c)}$ and it leads to a drop in the conductivity and a rise in the resistivity. Thus, in order to account for the temperature behavior in resistivity observed in the pseudogap state, the resistivity should be dominated by the contribution from the cold spots and that from the hot spots be negligible. Now, we return to our realistic calculation using the interaction form Eq.(3). From Fig.3, one finds that the ratio of the relaxation rate at the hot spots to that at the cold spots is about 4 (a band calculation gives the same ratio, see table II in Ref. [7]) and 7 for the dispersions (1) and (2), respectively. Thus, no overwhelming contribution from the cold spots can be expected just from this ratio. In this case, the kinematical factor (Fermi velocity v_F) should be considered, since the transport coefficients involve a k-sum over τ_k weighted by v_F^2. As noted above, for the dispersion (2) the ratio of the Fermi velocity at the cold spots (near k-point B) is 2.5 times larger than at the cold spots (near k-point A). This, along with the ratio 7 for the relaxation rate, makes $\sigma_{xx}^{(c)}$ at the k-point A be 44 times larger than $\sigma_{xx}^{(h)}$ at the k-point B and justifies the applicability of the cold spot model. However, for the dispersion (1) the Fermi velocity at the cold spots is nearly 1.15 times smaller than at the cold spots, consequently $\sigma_{xx}^{(c)}$ is only 3 times larger than $\sigma_{xx}^{(h)}$. Thus, the losing in $\sigma_{xx}^{(h)}$ due to the opening of the pseudogap will exceed the increase in $\sigma_{xx}^{(c)}$ arising from the enhancement in $\tau_k^{(c)}$ and eventually the resistivity will increase.

From the above discussion, one can see that the crossover behavior of the resistivity is better described by the cold spot rather than the hot spot model, which is consistent with the recent studies on the transport properties in the normal state [3,6]. In a realistic calculation, we find that the variation of the Fermi velocity along the FS plays an important role in the determination of the cold spot or hot spot model. In terms of the ARPES experiments [10,11], an extended van Hove singularity (flat band) exists near $(0, \pm\pi)$ — around the hot spots, it will lead to a lower Fermi velocity around the hot spot region and justifies the applicability of the cold spot model. However, the energy dispersion of Eq.(1) is not flat enough and meanwhile the flat band is far away from the FS. Consequently, it has larger Fermi velocity near the hot spots as shown in the inset of Fig.2. So, as far as our model is concerned, the dispersion (1) is inadequate for the description of the transport properties in the underdoped cuprates though it was used mostly before.

III. FITTING TO EXPERIMENTAL DATA

Although the agreement between the model calculation of the resistivity using the dispersion (2) and experiments is reasonable in view of its crossover behavior from the normal to the pseudogap state, there are two discrepancies when fitting it to experiments quantitatively. One is a non-linear temperature resistivity appears at high temperatures and the other is that the resistivity ceases to decrease and even has a slight rise with further decreasing temperature below about 100 K which is higher than T_c as can be seen in Fig.4(b). To resolve these discrepancies, we note that the bandstructure (2) is obtained from a fit to the photoemission experimental data of $Ba_2Sr_2CaCu_2O_8$ with hole doping 0.17, i.e., an optimally doped cuprate, so applying it to the underdoped regime by just adjusting its chemical potential is a rigid band assumption. In fact, the bandstructure will change as doping varies. An important fearure is that the band width will become narrow, i.e., the quasiparticles will becomes heavy as doping decreases. Of course, this renormalization of mass is anisotropic in momentum space, it is larger near the FS and becomes more and more less away from it. The detailed treatment of this renormalization requires a complicated calculation and goes beyond our scope here, thus we simply take $\varepsilon_k \to \varepsilon_k/3.0$. This amounts to reducing the energy difference between the chemical potential and the flat band for hole doping $n = 0.1$ from 54 meV to 18 meV, which is consistent with ARPES experimental data 19 meV for the underdoped $YBa_2Cu_4O_8$ [11]. The reduction of the whole energy band by a factor of 3 is justified approximately by the fact that just the electrons near the FS contribute to transports and those far away from it have in fact no effect. Before making a quantitative comparison with experiments, we note that Wuyts

et al. [2] have developed an universal analyzing method for transport data in underdoped high-T_c superconductors. They demonstrated that the transport data on $YBa_2Cu_3O_x$ can be scaled onto an universal curve using one scaling parameter T_0 which has $0.8T_0 \approx T^*$. We will adopt this method in the following analysis.

The results for the dc resistivity $\rho(T) = 1/\sigma_{xx}$, calculated using the dispersion (2) reduced by a factor of 3 with $\mu = 0.02t$ (n=0.1) and using the dispersion (2) but with $\mu = -0.016t$(the dashed-dotted line), are shown in Fig.5, where the residual resistence is taken to be $\rho_0 = 0.162\rho(T_0)$, the same value as used before [2], $T^* = 0.72T_0$ with $T^* = 150$K. The result represented by the dashed-dotted line has the same energy difference 18 meV to that calculated using the reduction of the bandwidth. The hollow squares indicate the experimental data of Ref. [2]. An important effect of the reduction of the energy band is that the flat region becomes large, so the slight rise in the resistivity below about 100 K observed in Fig.4(b) is removed and a continue decrease is obtained which fits the experimental data well. On the other hand, though having the same energy difference, the result by adjusting the chemical potential (dashed-dotted line) still shows a rise below 100 K. It implies that it is the range of the flat band instead of the difference between the chemical potential and the flat band that has something to do with the low temperature rise in resistivity. This may be understandable from the reason causing this rise. As the gapped regions spread with decreasing temperature, more and more parts of the FS are destroyed. Since the Fermi velocity increases when the wavevector moves from the k-point A to B, the ratio of the Fermi velocity at the cold spots to that at the crossing of the FS and the edge of the gapped regions will decrease. Thus, the contribution to the conductivity from the hot regions will grow gradually and the resistivity will cease to decrease or even rise in low temperatures. If we reduce the width of the energy band, then the range of the flat band and consequently the range of the low Fermi velocity will grow. It enables the contribution from the hot regions to be negligible. One can also see from the figure that a linear in T dependence is well reproduced in the normal state, although its slope is somewhat larger than experimental data. The results for different T-dependences of the radius of gapped regions $R(T)$ are shown in the inset of Fig.4. We find that the best fit to the experimental data is $R(T) \propto (T^* - T)$ though the difference between $R(T) \propto (T^* - T)^{1/2}$ and $R(T) \propto (T^* - T)$ is minor. The comparison of the resistivities calculated for the commensurate and incommensurate cases is also shown in Fig.5, in which the dashed line represents the result for the commensurate case. The qualitative difference between them is that the slop is smaller for the commensurate case and make the fit become bad. As noted above, the temperature dependence of the resistivity is determined by the weight of the contributions from the cold spots to that from the hot spots. The incommensurate wave vectors will make the hot spots be shifted away from the original ones (move to the cold spots for $-\delta\mathbf{Q}$ and to the boundary of the Brillouin zone for $\delta\mathbf{Q}$) and thus lead to a change of the weight of the contribution from the cold spots to that from the hot spots. It is this change that gives rise to different slops in the temperature behavior of the resistivity.

Using the same parameters, we have calculated the T-dependences of the inverse Hall angle $\cot\theta_H(T) = \sigma_{xx}/\sigma_{xy}$ and the Hall coefficient $R_H = \sigma_{xy}/B\sigma_{xx}\sigma_{yy}$. The result for the inverse Hall angle is presented in Fig.6. The fit to experimental data above T^* is good below about 300K. Below 150 K, a slight deviation from the T^2 appears, especially, the $\cot\theta_H(T)$ curve changes from convexity to concavity with nearly the same reflection point as the experimental data for the incommensuration case. Comparing the results for different T-dependences of the gapped regions, one can find that there is no significant difference as shown by the solid and dotted lines. The results for the commensurate case (dashed line) and calculated using the dispersion (2) with $\mu = -0.016t$(dashed-dotted line) all show disagreement with the experimental data at high temperatures and also exhibit a deviation from the high-T behavior at much low temperature compared with the experiment.

As for the Hall coefficient shown in Fig.7, we obtain a weaker temperature dependence than that seen experimentally [1,2]. The similar result has been reported by Stojkovic and Pines based on the NAFL model [5]. However, the trend is very similar to the experimental data and allows us to compare its crossover behavior with the experiment qualitatively. A striking feature for the incommensuration cases which are represented by the solid and dotted lines is that the Hall coefficient decreases rapidly with decreasing temperature at low temperatures and causes a peak occurring slightly below the opening temperature T^*. This is qualitatively consistent with experiments [1,2]. We note that the result with commensuration (dashed line) shows an even weaker T dependence than the case of incommensuration. Moreover, the results calculated using the dispersion (2) with $\mu = -0.016t$(dashed-dotted line) displays a contrary temperature behavior, i.e., it decreases with temperature. This strong discrepancy is related to the discrepancy in the resistivity discussed above. Because $R_H \propto 1/\sigma_{xx}^2$, any slight deviation from the T-linearity in $\rho(T)$ will be amplified and leads to a worse result for the Hall coefficient. From the same arguement as that for resistivity, we know that the main contribution to the transverse conductivity σ_{xy} comes from the cold spots and the hot spots contribute little [3]. So, σ_{xy} will have the same trend as that for the longitudinal conductivity σ_{xx}, and their effect will cancel and lead to a minor variation in the temperature dependence of the inverse Hall angle. On the other hand, the depression will reflect in the Hall coefficient since we have $R_H = \sigma_{xy}/B\sigma_{xx}\sigma_{yy}$.

This agreement with experiments using the dispersion (2) reduced by a factor of 3 raises a question: whether the dispersion (1) also works after the same reduction. We have done it and the result turns out to be bad. The reason is that there is another vH singularity in the dispersion (1) except that at $(0, \pi)$, it exists at $(0, 0)$ point. That part

of the FS near the diagonal direction will approach to this one when the energy band is reduced and increase the density of states at the cold spots, eventually this will change the weight of cold spots to hot spots drastically.

IV. DISCUSSION AND CONCLUSION

In summary, we have investigated the effect of the FS destruction on transport properties in the pseudogap state of underdoped high-T_c cuprates based on the standard Boltzmann theory. Using a simple assumption of taking the density of states of the gapped regions to be zero, we calculate the temperature dependences of the longitudial resistivity, the Hall angle and the Hall coefficient. The results indicate that the temperature dependence of the transport coefficients is strongly sensitive to the existance and the range of the flat band near $(0, \pm\pi)$, and the anistropy of the scattering rates for electrons along the Fermi surface. We find that the temperature dependences of the transport coefficients in the pseudogap state are better described by the cold spot model, i.e., they are determined by the contribution from the cold spots while the hot spots contribute little. We can semi-quantitatively explain the temperature dependences of both the resistivity and the Hall angle, as well as qualitatively explain the crossover behavior of the Hall coefficient from the normal state to the underdoped state. However, the calculated Hall coefficient in the normal state shows a weaker temperature dependence than that observed by experiments.

It is worthwhile to point out that in NAFL model the different magnetic properties in underdoped systems are ascribed to distinct scaling regimes of the spin-fluctuation spectrum Eq.(2) [17]. From this point of view, the anomalous transport properties may arise from the different interaction form which is related to the opening of the "spin pseudogap" as deduced from the NMR and neutron scattering experiments [18], though there is no detailed calculations about it now. Here, we focus on the effect of the Fermi surface topology and consider the interaction form in the underdoped regime to be the same as that in the optimally doped regime. What is the relation between the two proposals and also if any other interaction form which gives a varying electron lifetime on the FS such as Eq.(2) can give the same results presented here deserve further investigations.

ACKNOWLEDGMENTS

We would like to thank M.R.Norman for discussion and for pointing out the dispersion Eq.(2). We acknowledge the support from NSC of Taiwan under Grants No.88-2112-M-001-004 and No.88-2112-M-003-004. JXL is support in part by the National Nature Science Foundation of China.

* On leave from Department of Physics, Nanjing University, Nanjing 210093, People's Republic of China

---

[1] T.Ito, K.Takenaka, and S.Uchida, **70**, 3995 (1993); B.Bucher, P.Steiner, J.Karpinski, E.Kaldis, and P.Wachter Phys. Rev. Lett.**70**, 2012 (1993); T.Watanabe, T.Fujii, and A.Matsuda, **79**, 2113 (1997).

[2] B.Wuyts, V.V.Moshchalkov, and Y.Bruynseraede, Phys. Rev. B **53**, 9418 (1996); V.V.Moshchalkov, cond-mat/9802281 (unpublished).

[3] See, B.P.Stojkovic and D.Pines, Phys. Rev. B**55**, 8576 (1997) and references therein.

[4] R.Hlubina and T.M.Rice, Phys. Rev. B**51**, 9253 (1995).

[5] B.P.Stojkovic and D.Pines, Phys. Rev. Lett.**76**, 811 (1996).

[6] L.B.Ioffe and A.J.Millis, Phys. Rev. B**58**, 11631 (1998).

[7] A.T.Zheleznyak, V.M.Yakovenko, H.D.Drew, and I.I.Mazin Phys.Rev.B**57**, 3089 (1998); J.Paaske and D.V.Khveshchenko Phys.Rev.B**57**, R8137 (1998);

[8] See reviews B.Batlogg *et.al.*, Physica C**235-240**, 130 (1994) and M.Randeria, cond-matt/9710223 (unpublished).

[9] M.R.Norman *et al.*, Nature **392**, 1571 (1998).

[10] Z.X.Shen and D.Dessau, Phys. Rep. **253**, 1 (1995); D.Dessau *et al.*, Phys. Rev. Lett. **71**, 2781 (1993).

[11] K.Gofron *et al.*, Phys. Rev. Lett. **73**, 3302 (1994).

[12] P.Monthoux and D.Pines, Phys.Rev.B **49**, 4261 (1994).

[13] P.A.Lee, N.Nagaosa, T.K.Ng, and X.G.Wen, Phys. Rev. B **57**, 6003 (1998); V.J.Emery and K.A.Kivelson, Nature **374**, 434 (1996); H.Fukuyama, H.Kohno, and T.Tanamoto, J. Low Temp. Phys. **95**, 309 (1994); B.Janko, J.Maly, and K.Levin, Phys. Rev. B **56**, R11 407 (1997).

[14] N.Furukawa, T.M.Rice, and M.Salmhofer, Phys. Rev. Lett. **81**, 3195 (1998).

[15] V.B.Geshkenbein, L.B.Ioffe, and A.I.Larkin, Phys. Rev. B**55**, 3173 (1997).
[16] P.Dai, H.A.Mook, and F.Dogan, Phys. Rev. Lett. **80**, 1738 (1998); In this paper, the incommensurate peaks are reported to lie along the diagonals. But, it has been changed to along the Brillouin zone boundary in their later paper: H.A.Mook, P.Dai, R.D.Hunt, and F.Dogan, cond-mat/9712326 (unpublished).
[17] V.Barzykin and D.Pines, Phys. Rev. B **52**, 13 585 (1995);
[18] M.Takigawa *et al.*, Phys. Rev. B **43**, 247 (1991); J.Rossat-Mignod *et al.*, Physics C **185-189**, 86 (1991).

FIGURE CAPTIONS

Fig.1 Fermi surfaces for the dispersions (1) (dashed line) and (2) (thin solid line) with hole doping $n = 0.1$. The thick solid lines enclose the "disk" regions where a pseudogap is suggested by experiments. The density of states of electrons in that regions will be assumed to be zero in our model calculations.

Fig.2 Energy dispersions for Eqs.(1) and (2) described in the text along the $\Gamma = (0,0)$ — $\mathrm{M} = (0,\pi)$ — $\mathrm{Y} = (\pi,\pi)$ direction. Note the very flat band existing near M for Eq.(2). The inset shows the Fermi velocities along Fermi surface for the dispersions (1) (dotted line) and (2) (solid line). The k-point A', B and A corresponds to what indicated in Fig.1.

Fig.3 Relaxation rates as a function of temperature at different k points along the Fermi surface. (a) and (b) are the results calculated using Eq.(1), (c) and (d) are those using Eq.(2). The k-point symbols (A and B) correspond to what indicated in Fig.1. The maximum value of the radius of the gapped region is $R_{max} = 0.25\pi$(see text) and their T-dependences are $R(T) \propto (T^* - T)$(solid lines), $(T^* - T)^{1/2}$ (dashed lines) and $\tanh(2\sqrt{T^*/T - 1.0})$(dotted lines). The results are for the commensurate magnetic interaction, those for the incommensuration case are qualitatively similar to the results shown here except for a larger values.

Fig.4 Sensitivity of the resistivity with respect to the dispersions (1) [(a)] and (2) [(b)]. The solid line indicates the result with a T-dependence of the radius of the gapped region $R(T) \propto \tanh(2\sqrt{T^*/T - 1.0})$, the dashed line with $R(T) \propto (T^* - T)$, and both correspond to the maximum value $R_{max} = 0.25\pi$. The dotted line corresponds to the case of $R_{max} = 0.3\pi$ and $R(T) \propto (T^* - T)$. For comparison, we also show the result for the commensuration case as indicated in the figure.

Fig.5 Scaled resistivity versus scaled temperature with the maximum value of the radius of the gapped region $R_{max} = 0.3\pi$. The solid, dashed, dotted lines and those in the inset are the results calculated using the dispersion (2) reduced by a factor of 3. The dashed-dotted line is the result calculated using the dispersion (2) with the chemical potential $\mu = -0.016t$ (see text). Solid line: the T-dependence of the radius of the gapped region $R(T) \propto (T^* - T)$, the incommensuration $\delta Q = 0.12\pi$. Dashed line: $R(T) \propto (T^* - T)$, $\delta Q = 0$. Dotted line: $R(T) \propto (T^* - T)^{1/2}$, $\delta Q = 0.12\pi$. Dashed-Dotted line: $R(T) \propto (T^* - T)$, $\delta Q = 0.12\pi$. The open squares, both in the main panel and in the inset, are experimental data from Ref. [2]. Inset shows the sensitivity of the resistivity with respect to the size and temperature dependence of the gapped region. Solid line: the same parameters with the solid line in the main panel. Dashed line: $R(T) \propto (T^* - T)$, $R_{max} = 0.25\pi$. Dotted line: $R(T) \propto \tanh(2\sqrt{T^*/T - 1.0})$, $R_{max} = 0.25\pi$.

Fig.6. Scaled inverse Hall angle versus scaled temperature with the maximum value of the radius of the gapped region $R_{max} = 0.3\pi$. The solid, dashed and dotted lines are the results calculated using the dispersion (2) reduced by a factor of 3. The dashed-dotted line is the result calculated using the dispersion (2) with the chemical potential $\mu = -0.016t$ (see text). Solid line: the T-dependence of the radius of the gapped region $R(T) \propto (T^* - T)$, the incommensuration $\delta Q = 0.12\pi$. Dashed line: $R(T) \propto (T^* - T)$, $\delta Q = 0$. Dotted line: $R(T) \propto (T^* - T)^{1/2}$, $\delta Q = 0.12\pi$. Dashed-Dotted line: $(T^* - T)$, $\delta Q = 0.12\pi$. The open squares are experimental data from Ref. [2].

Fig.7. Temperature dependence of the Hall coefficient with the maximum value of the radius of the gapped region $R_{max} = 0.3\pi$. The solid, dashed and dotted lines are the results calculated using the dispersion (2) reduced by a factor of 3. The dashed-dotted line is the result calculated using the dispersion (2) with the chemical potential $\mu = -0.016t$ (see text). Solid line: the T-dependence of the radius of the gapped region $R(T) \propto (T^* - T)$, the incommensuration $\delta Q = 0.12\pi$. Dashed line: $R(T) \propto (T^* - T)$, $\delta Q = 0$. Dotted line: $R(T) \propto (T^* - T)^{1/2}$, $\delta Q = 0.12\pi$. Dashed-Dotted line: $(T^* - T)$, $\delta Q = 0.12\pi$.

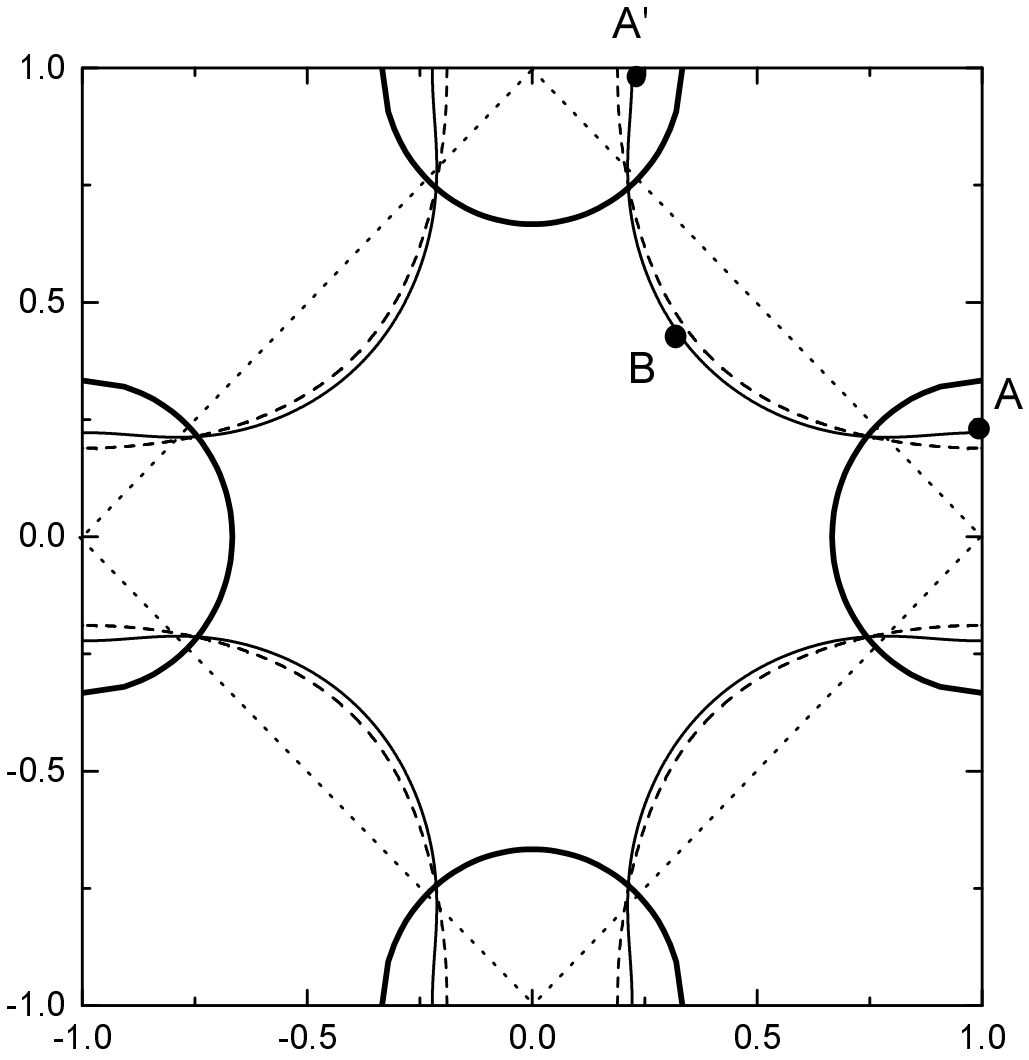

Fig. 1 Li, Wu and Lee

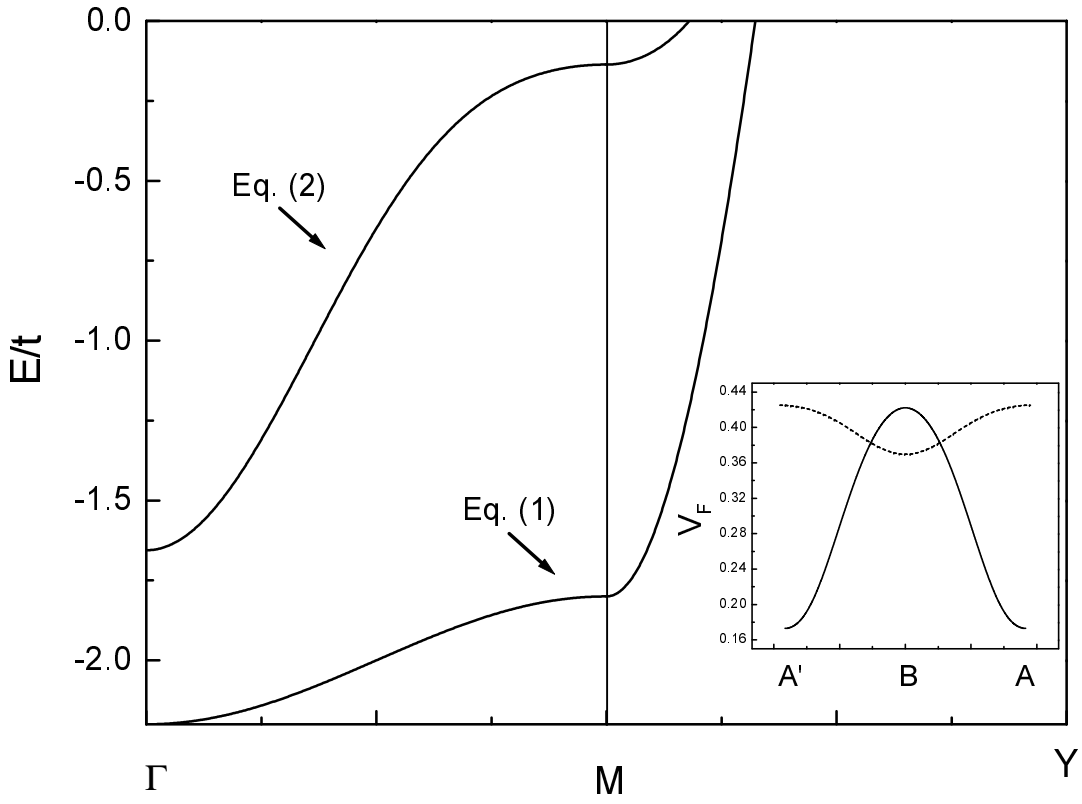

Fig.2 Li, Wu and Lee

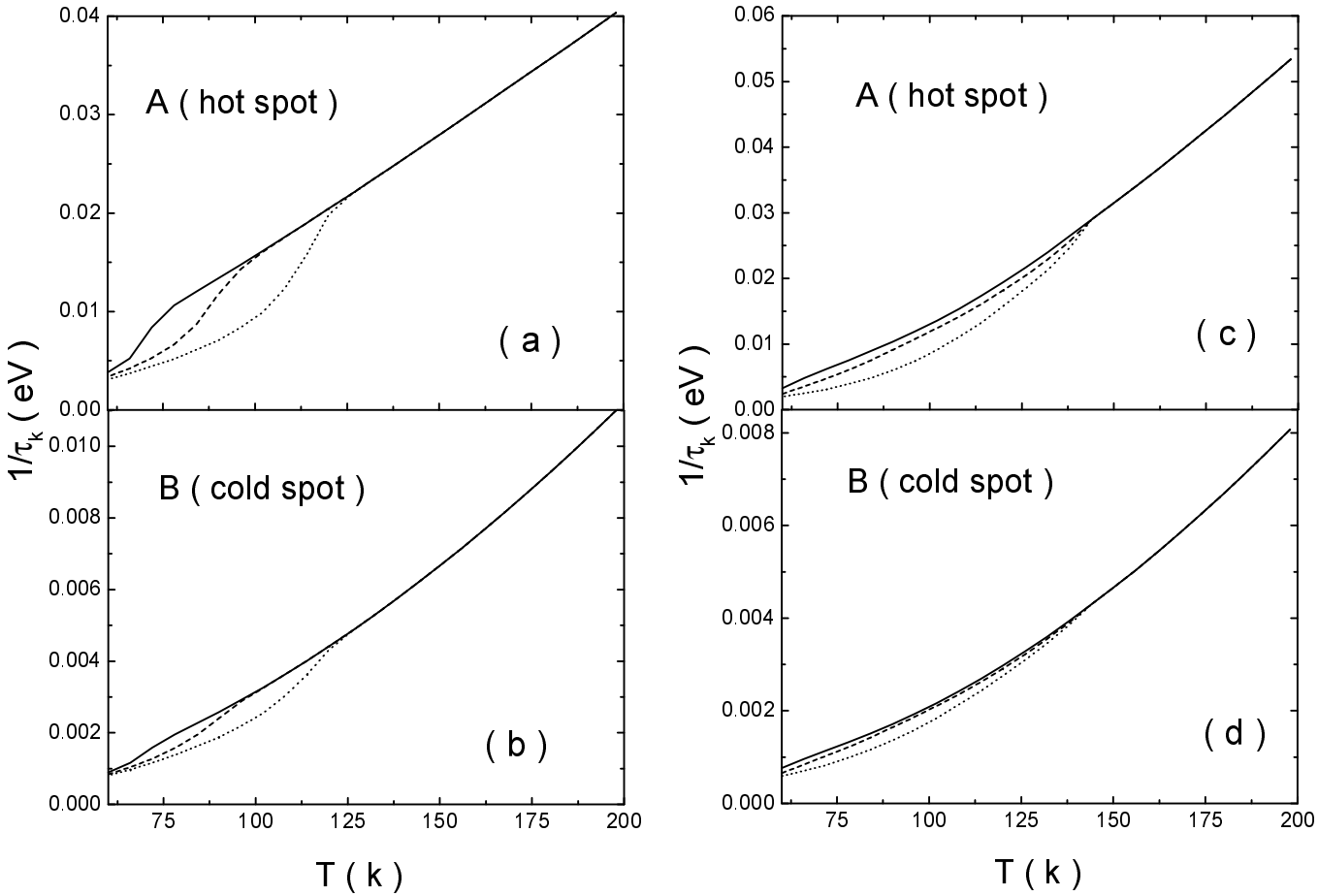

Fig.3 Li, Wu and Lee

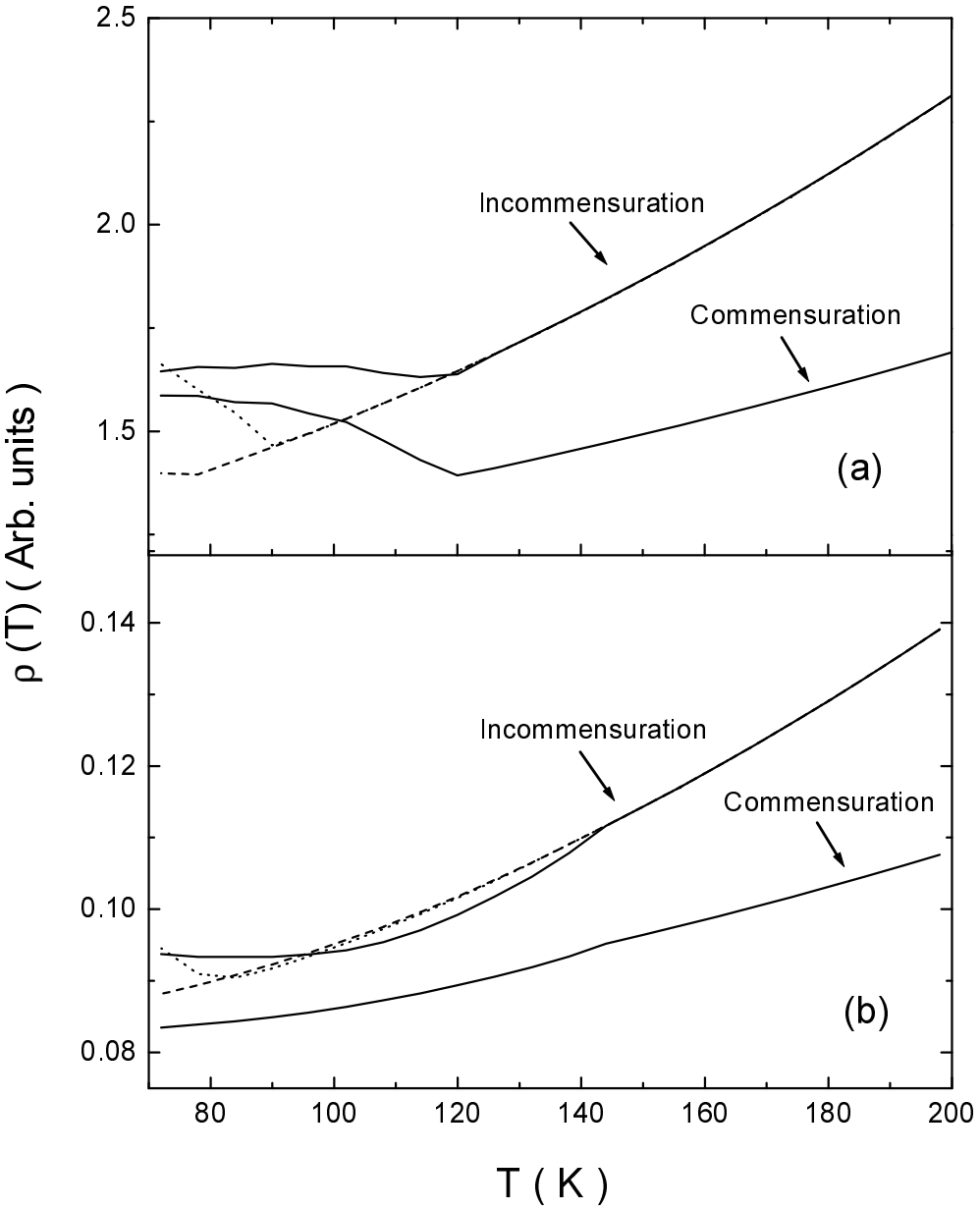

Fig. 4 Li , Wu and Lee

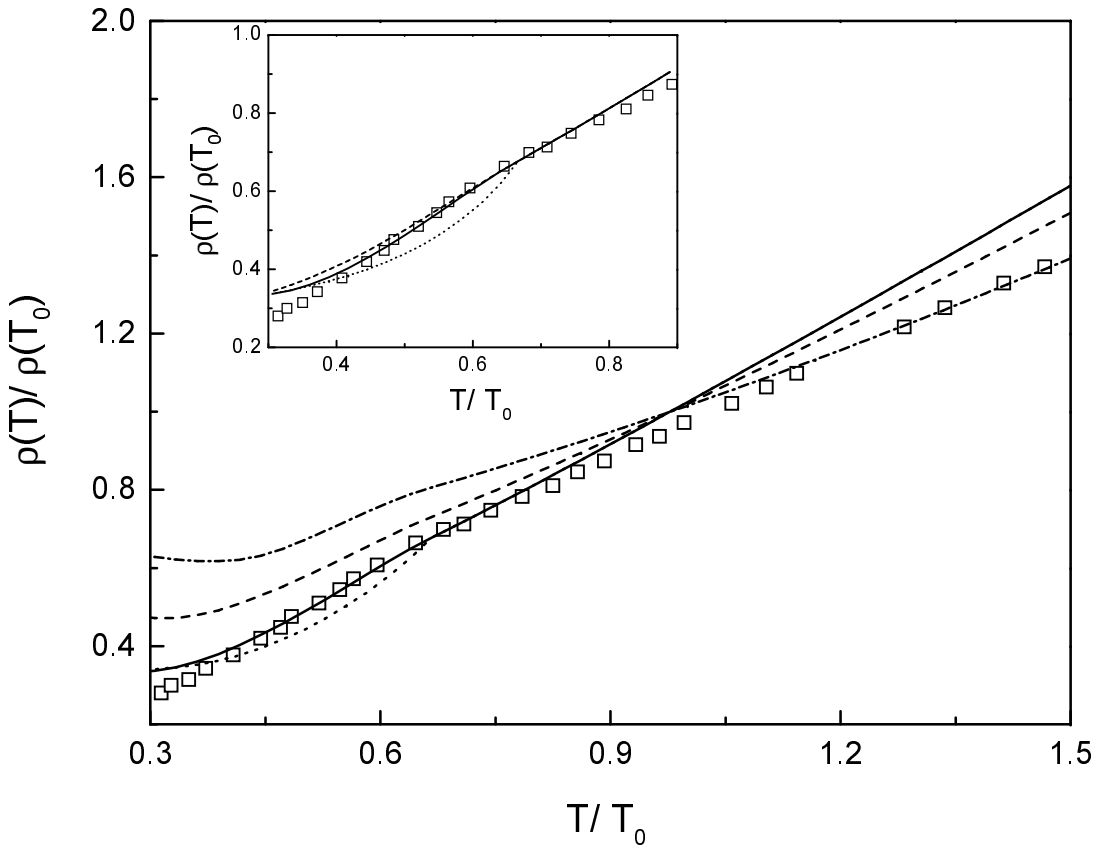

Fig.5 Li, Wu and Lee

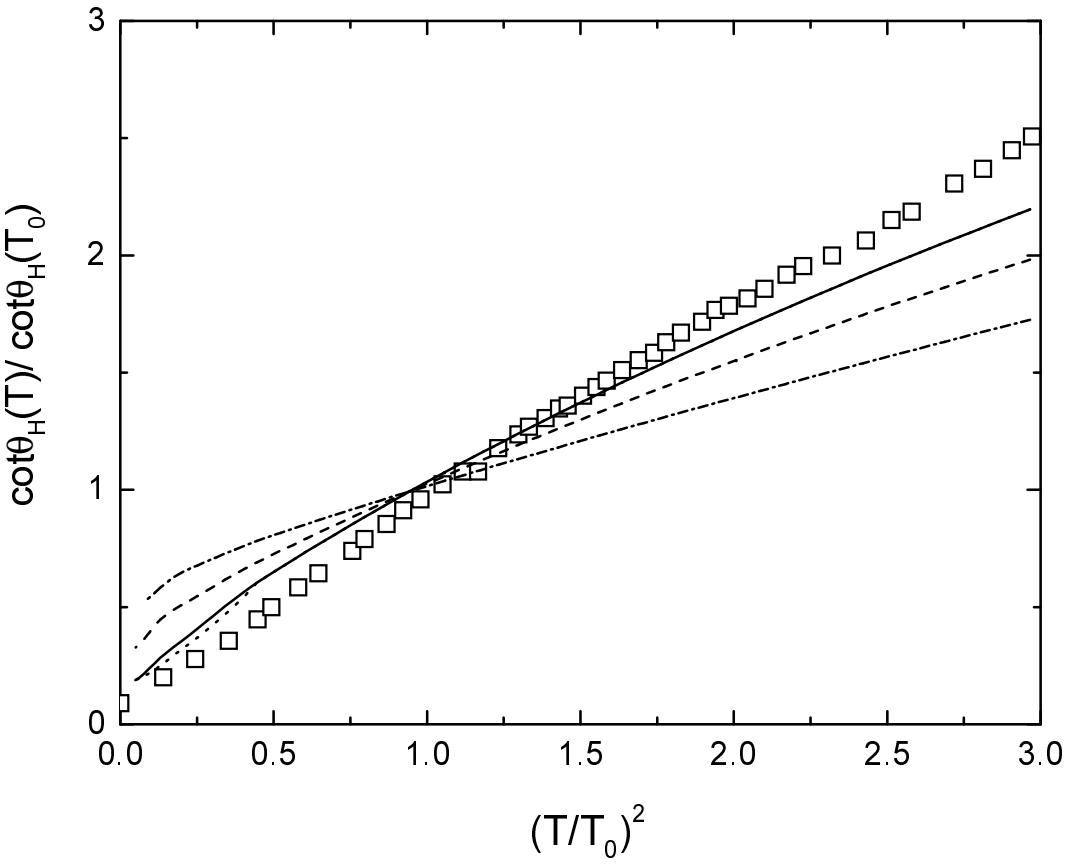

Fig.6 Li, Wu and Lee

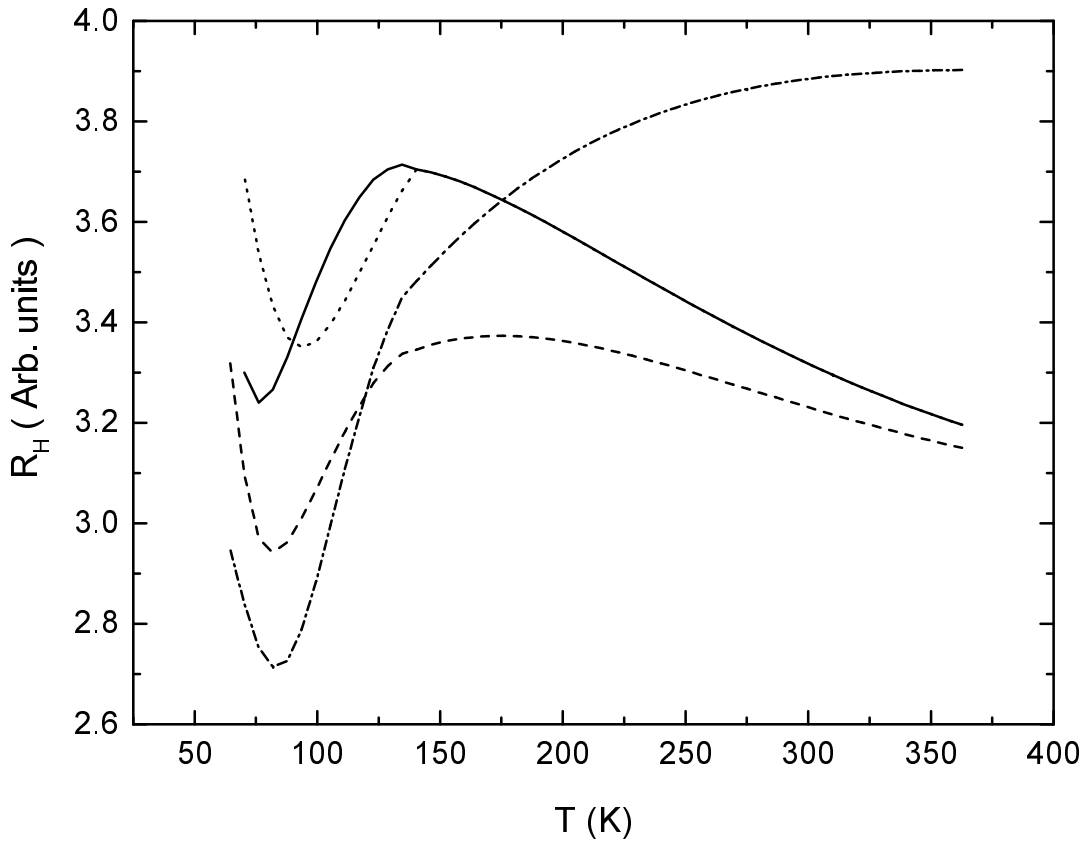

Fig.7 Li, Wu and Lee